J. Opt. Commun. 24 (2003) 895,

Journal of Optical Communications

Analysis of high speed Traveling-Wave Electrooptic $LiNbO_3$ Devices based on a 3-D Integral Method

A. Chipouras, T. Sphicopoulos (member IEEE), D. Varoutas (student member IEEE)

Summary

Electrooptic devices (modulators and switches) with travelling wave electrodes are important elements of broadband optical networks. A general simulation model with results being in a good agreement with experimental ones is developed. A 3-D integral method is used in order to determine the microwave electrode parameters with high accuracy. Assuming a simplified refractive index profile for the diffused optical waveguide, an analytical approach of the fundamental optical mode is obtained. The model proves to be an efficient tool for the design and optimisation of broadband electrooptic devices with low drive power requirement.

1 Introduction

Today's telecommunications market highly driven by IP-oriented applications demands more transport capacity. This fact leads to the increasing use of optical networks with multiplexing techniques such as WDM, to exploit the bandwidth of the optical support media. The implementation of these networks is mainly based on high speed optical modulation and switching. Components made of Titanium diffused Lithium Niobate (Ti:$LiNbO_3$), Indium Phosphide multiple quantum wells (MQW) and electro-optic polymer, are widely used in digital communication systems operating at 2.5 and 10 Gb/s and in analog cable TV. Among them the Ti:$LiNbO_3$ devices are the most promising to satisfy the trend for even higher bandwidth. Their advantages include efficient coupling with optical fibers, high electrooptic coefficients, low dc drift, very small frequency chirp and of course high operational speed with travelling wave electrodes (TW).

In this paper an integral method (IM) is used to calculate the microwave parameters of structures with coplanar electrodes on a stratified medium, including anisotropic layers. Since the transverse dimensions of the electro-optic devices are much smaller than the microwave wavelength, the assumption of quasi-static behaviour is made. Consequently the relevant 3-D Green function is obtained by solving the corresponding Poisson equation with the appropriate boundary conditions. The quasi-static approximation requires less computational effort giving reasonable results since the dispersion effects are small for coplanar electrodes up to the frequency of 40 GHz [1]. The behaviour at high frequencies is considered by assuming the equivalent to the electrodes transmission line, with distributed parameters those that have been calculated by the static approach. The electrode thickness is taken into account by a simple (but accurate enough for design purposes) closed form approximation, which, in the other hand simplifies the estimation of the conductor losses of the electrodes by the Incremental Inductance Formula.

As singlemode Ti diffused waveguides are used in practice, only the fundamental optical mode is considered. Assuming a parabolic refractive index profile for the optical waveguide after the diffusion, the wave equation is solved analytically. The obtained mode profile with parameters directly connected to diffusion conditions is used to calculate the overlap factor between the microwave field and the optical mode. In this manner computational effort required by other methods (e.g. Finite Elements-FEM) is avoided.

The accuracy of the model was established by comparison with experimental results of practical electrooptic devices found in the literature. Finally, optimized parameters of electrooptic devices with 20 GHz bandwidth and low drive power are presented.

2 Electrical parameters calculation

In general, an electrooptic device consists of ν metallic contacts on the top of a stratified dielectric material and is similar to microstrip structures. There are several methods [1, 2, 12] available for modeling these devices. One of the most general and rigorous treatment is given

Address of authors:

1 Department of Informatics and Telecommunications
of the University of Athens
Panepistimiopolis, GR-157 84, Athens, Greece
A. Chipouras: Tel.: (+30210) 7275319
E-mail: aris@di.uoa.gr
Fax: +(30210) 7275601
Thomas Sphicopoulos: Tel.: +(30210) 7275313
E-mail: Th.Sfikopoulos@di.uoa.gr
D. Varoutas: Tel.: +(30210) 7275313
E-mai: arkas@di.uoa.gr

Received ●●●●

Journal of Optical Communications
24 (2003) 895

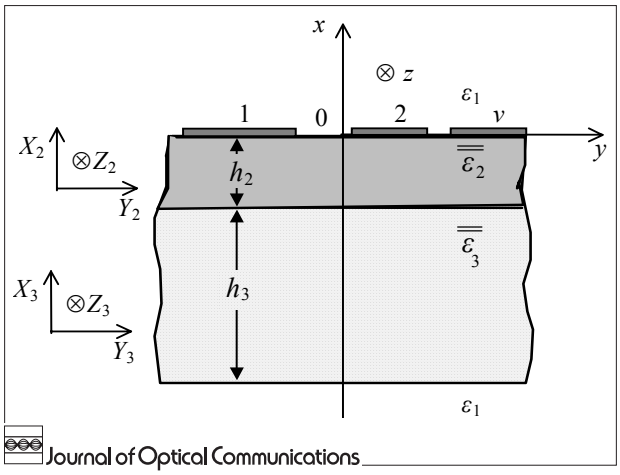

Fig. 1: Schematic cross section of a general electrooptic structure with several coplanar electrodes on top of a layered dielectric substrate

by the well-known Integral Equation Method (IM), usually formulated in the spectral domain.

In this paper a quasi-static approach of IM is used, since the transverse dimensions of the electrooptic device (~100 μm) are much smaller than the wavelength (~10^3–10^7 μm) of the electric control wave applied on the contacts.

Assuming that V_i is the static potential applied on each electrode i = 1,2…ν, the integral equation for the corresponding total charge density $\sigma(\vec{\rho}'_j)$ follows as:

$$V_i = \sum_{i=1}^{\nu} \int\int_{s_j} G_o(\rho)\sigma(\vec{\rho}'_j)\,dS \tag{1}$$

S_i is the surface of each electrode and $G_0(\rho)$ the Green function calculated in the interface where the electrodes are placed. Green function corresponds physically to the potential created at the point $\vec{r}$ by a unit point source at $\vec{\rho}'_j$ with ρ the source-observer distance on the plane of electrodes.

Green function is evaluated by considering a general case of an electrooptic structure with the cross section shown in Fig. 1. The metallic contacts on the top of the stratified dielectric material are assumed to be infinitely thin and perfectly conducting, extended parallel to the ±z direction with finite length L. The total structure consists of four layers. The top and the lower layers are isotropic with dielectric constant ε_1 (usually air) and infinitely extended in the ±x directions. The remaining layers underneath the electrodes plane of thickness h_i, (i = 2, 3) are assumed to consist of anisotropic uniaxial crystals with their crystallographic axes $[X_i, Y_i, Z_i]$ lined up along the directions of the coordinates system [x, y, z] in use. Their dielectric properties can be characterized by the diagonal dielectric tensor: $\bar{\bar{\varepsilon}}_i = [\varepsilon_{xi}, \varepsilon_{yi}, \varepsilon_{zi}]$ i = 2, 3.

Green function in each dielectric region is derived by matching the solutions in the different layers of Poisson equation in the spectral domain [3]. Nevertheless, working in the space domain helps us to keep a good physical insight of the problem. Hence, by using the inverse Fourier transform, the spatial Green function in each layer of interest has the following form:

• $x \geq 0$

$$G_1(x|\rho,\theta) = \frac{1}{(2\pi)^2\varepsilon_0}\int_0^{2\pi}\int_0^{\infty} A(\xi,\varphi,\varepsilon_{\varphi i},h_i)e^{-\xi x}d\xi d\varphi \tag{2a}$$

• $-h_2 \leq x \leq 0$

$$G_2(x|\rho,\theta) = \frac{1}{(2\pi)^2\varepsilon_0}\int_0^{2\pi}\int_0^{\infty} B(\xi,\varphi,\varepsilon_{\varphi i},h_i)\sinh(\xi\varepsilon_{\varphi 2}x)d\xi d\varphi + \frac{1}{(2\pi)^2\varepsilon_0}\int_0^{2\pi}\int_0^{\infty} A(\xi,\varphi,\varepsilon_{\varphi i},h_i)\cosh(\xi\varepsilon_{\varphi 2}x)d\xi d\varphi \tag{2b}$$

• $-(h_2 + h_3) \leq x \leq -h$

$$G_3(x|\rho,\theta) = \frac{1}{(2\pi)^2\varepsilon_0}\int_0^{2\pi}\int_0^{\infty} C(\xi,\varphi,\varepsilon_{\varphi i},h_i)\sinh\left[\xi\varepsilon_{\varphi 3}(x+h_2+h_3)\right]d\xi d\varphi \tag{2c}$$

Where ξ and φ are dummy spectral variables [3] and:

$$\begin{aligned} y - y' &= \rho\cos\theta \\ z = z' &= \rho\sin\theta \end{aligned} \tag{3a}$$

$$\left.\begin{aligned} A(\xi,\varphi,\varepsilon_{\varphi i},h_i) &= g(\xi,\varphi)\left[\tanh(\xi\varepsilon_{\varphi 3}h_3) + \frac{\varepsilon_{x\varphi 3}}{\varepsilon_{x\varphi 2}}\tanh(\xi\varepsilon_{\varphi 2}h)\right] \\ B(\xi,\varphi,\varepsilon_{\varphi i},h_i) &= g(\xi,\varphi)\left[\tanh(\xi\varepsilon_{\varphi 2}h_2)\tanh(\xi\varepsilon_{\varphi 3}h_3) + \frac{\varepsilon_{x\varphi 3}}{\varepsilon_{x\varphi 2}}\right] \\ C(\xi,\varphi,\varepsilon_{\varphi i},h_i) &= \frac{g(\xi,\varphi)}{\cosh(\xi\varepsilon_{\varphi 2}h_2)\cosh(\xi\varepsilon_{\varphi 3}h_3)} \end{aligned}\right\} \tag{3b}$$

$$g(\xi,\varphi) = e^{j\xi\rho\cos\varphi}\Big/\left[\varepsilon_1 + \varepsilon_{x\varphi 2}\tanh(\xi\varepsilon_{\varphi 2}h_2)\right]\tanh(\varepsilon_{\varphi 3}h_3) + \frac{\varepsilon_{x\varphi 3}}{\varepsilon_{x\varphi 2}}\left[\varepsilon_1\tanh(\xi\varepsilon_{\varphi 2}h_2) + \varepsilon_{x\varphi 2}\right] \tag{3c}$$

$$\left.\begin{aligned} \varepsilon_{x\varphi i} &= \varepsilon_{xi}\varepsilon_{\varphi i} \\ \varepsilon_{\varphi i} &= \sqrt{\frac{\varepsilon_{yi}+\varepsilon_{zi}}{2\varepsilon_{xi}}\left[1 + \frac{\varepsilon_{yi}-\varepsilon_{zi}}{\varepsilon_{yi}+\varepsilon_{zi}}\cos 2(\varphi+\theta)\right]^{1/2}} \end{aligned}\right\} i = 2,3 \tag{3d}$$

The above general expressions of Green function are applicable in many practical electrooptic devices which commonly use coplanar waveguides (CPW, ν = 3), asymmetric or symmetric coplanar strips (ACPS or SCPS, ν = 2) on X-cut or Y-cut (equivalently X-cut) $LiNbO_3$ substrates with thickness h and $\varepsilon_X = \varepsilon_Y = 28$ and $\varepsilon_X = 44$. The crystal cut, i. e. the orientation of its crystallographic axes relatively to the electrode plane and the position of the optical waveguides are chosen so that the higher electrooptic coefficient r_{33} can be utilized in all cases.

In the Z-cut devices the optical waveguides are positioned just bellow the edges of the electrodes, while a thin SiO_2 buffer layer with permittivity ε_s and thickness h_s, is used to minimize optical losses due to the metal contacts. The corresponding Green function, arises from the relations (2) and (3) setting $h_2 = h_s$, $h_3 = h$, $\varepsilon_1 = 1$, $\varepsilon_{x2} = \varepsilon_{y2} = \varepsilon_{z2} = \varepsilon_s$, $\varepsilon_{x3} = \varepsilon_Z$ and $\varepsilon_{y3} = \varepsilon_{z3} = \varepsilon_X = \varepsilon_Y$. In the Y-cut devices the optical waveguides are placed just between the electrodes and the buffer layer is not necessary. The corresponding Green function arises again from (2) and (3) setting $h_2 = h$, $h_3 \to \infty$, $\varepsilon_1 = 1$, $\varepsilon_{x2} = \varepsilon_{z2} = \varepsilon_Y$, $\varepsilon_{y2} = \varepsilon_Z$ and $\varepsilon_{x3} = \varepsilon_{y3} = \varepsilon_{z3} = 1$. The anisotropic nature of the electrooptic substrate is expressed by the θ dependence of the Green function through the relation (3c). It is obvious that this dependence vanishes in the case of the Z-cut devices, since $\varepsilon_{y3} = \varepsilon_{z3}$. This fact explains the common treatment of the electrooptic substrate as isotropic, independently of its cut with effective dielectric constant $\varepsilon_r = (\varepsilon_x\varepsilon_y)^{1/2}$ combined with a scaling of the x coordinate as $x' = x(\varepsilon_y/\varepsilon_x)^{1/2}$. However this approximation is far from true in the case of the Y-cut devices, where $\varepsilon_{y3} \neq \varepsilon_{z3}$. This considerable difference between the usual electrooptic devices in relation to the orientation of their anisotropic substrate is taken into account only by a 3-D approach.

Once the Green function for each case is evaluated, the integral equation (1) with,

$$G_0(\rho) = G_1(x|\rho)\big|_{x\to 0^+} = G_2(x|\rho)\big|_{x\to 0^-} \tag{4}$$

is solved and the electrodes charge density is determined. The solution is accomplished numerically by the widely used method of moments with subsectional basis functions. The charge density is expanded as:

$$\sigma(y,z) = \sum_{i=1}^{N_0} c_i f_i(y,z) \tag{5a}$$

where c_i are unknown coefficients, $N_0 = \sum_{i=1}^{\nu} N_i$

with N_i the number of rectangular subsections into which each electrode is divided and $f_i(y, z) = f_{iy}(y) \cdot f_{iz}(z)$ the corresponding basis functions.

These functions are chosen in such a way that they can fulfill the physical constraints of the problem, that is, the discontinuity of the charge density along the edges of the contacts.

Consequently the basis functions should have the form:

$$f_i(y,z) = f_{iy}\left(\left[1-\left(\frac{2y}{w_j}\right)\right]^{1/2}\right) f_{iz}\left(\left[1-\left(\frac{2z}{L}\right)^2\right]^{1/2}\right) \tag{5b}$$

w_j being the width of each electrode and $i = 1, 2 \ldots N_0$, $j = 1, 2 \ldots \nu$.

Replacing (5) into (1) and imposing the resulting equation to be satisfied at a discrete number N_0 of points in the surface of the electrodes (point matching), the integral equation is transformed into a $N_0 \times N_0$ linear system, resolved by trivial numerical methods. Results of the charge density are illustrated in Fig. 2, where symmetric electrodes (width w and interlectrode distance s) are assumed on a Y-cut substrate.

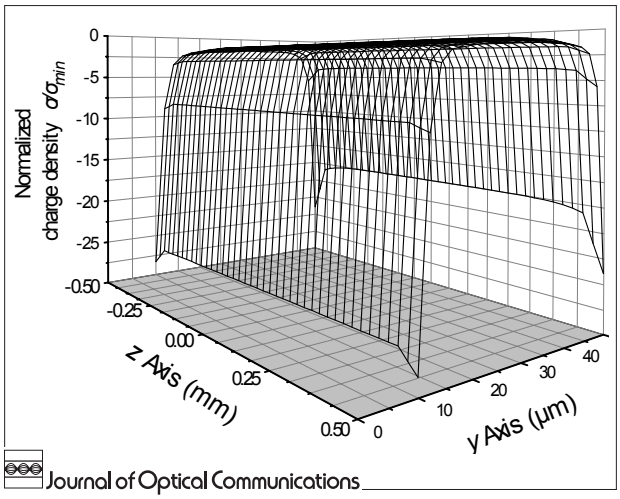

Fig. 2: Normalized surface charge density on the negative electrode of a electrooptic phase modulator (SCPS, Y-cut). s/w = 0.5, σ_{min} = 10.52 μCb/m^2, L = 1 mm and h = 0.5 mm

Once the charge density on the electrodes is known, the electric potential $\Phi_i(\vec{r})$ in every layer i of the structure is obtained from:

$$\Phi_i(\vec{r}) = \oint_{[S_v]} G_i(\vec{r}|\vec{\rho}')\sigma_S(\vec{\rho}')\,dy'dz' \qquad i = 1,2,3 \tag{6a}$$

The above integration is performed numerically on the surface $[S_v]$, which includes all the electrodes. The corresponding electric field vector $\vec{E}(\vec{r})$ in each region is given by:

$$\vec{E}_i(\vec{r}) = -\nabla\Phi_i(\vec{r}) \tag{6b}$$

In Figure 3 the electric field distributions $E_x(x, y, z)$ and $E_y(x, y, z)$ are depicted on the [x, y] plane in the middle of the SPCS electrodes. The presence of a sharp peak near the edges of the electrodes is noted. As it will be explained later, this peak does not influence the operational characteristics of the device significantly.

The lateral electric distribution remains nearly constant along the z-direction except for a region around the end of the electrodes (Fig. 4). In addition the E_z component remains nearly zero except the regions near the electrodes edges. However its magnitude is much lower compared to E_x and E_y and as a result its influence (small rotation of the crystal indicatrix trough the electrooptic coefficients r_{51} and r_{22}) is omitted. This fact testifies that the TEM approach widely used in the electrode analysis is a really good approximation.

A further investigation of the electric field distribution dependence on the electrodes structural parameters, that is the electrode gap s, the signal electrode width w and the thickness of buffer layer h_s can be performed by the Integral Method (IM). Concluding, it seems that the electric field in the Z-cut substrates is more directed along the depth direction, while in Y-cut, this is more oriented towards the lateral directions for all the electrodes configurations. The E_x component of electric field depends on $1/\sqrt{s}$, while the E_y on 1/s. The width of the electrodes

Journal of Optical Communications
24 (2003) 895

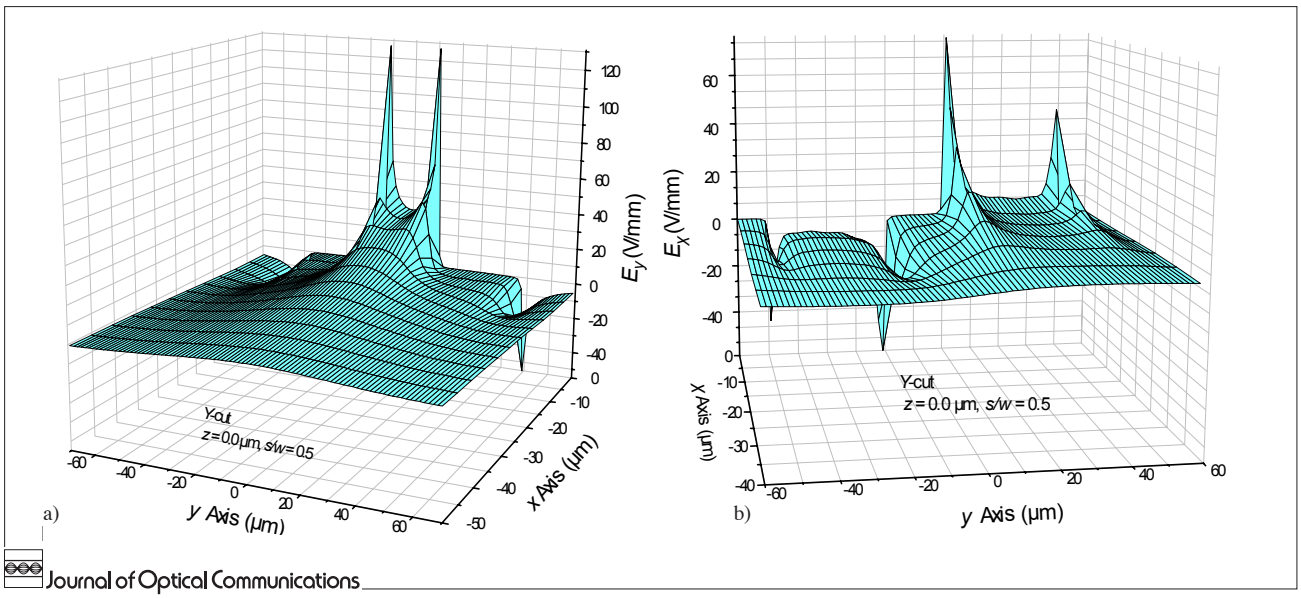

Fig. 3: Electric field distributions a) $E_y(x,y,z)$ and b)$E_x(x,y,z)$ on the plane [z = 0] of an electrooptic phase modulator (SCPS, Y-cut), for a difference voltage between the electrodes ΔV = 1 V (w = 40 μm, h_s = 0.0 μm L = 10 mm, h = 0.5 mm)

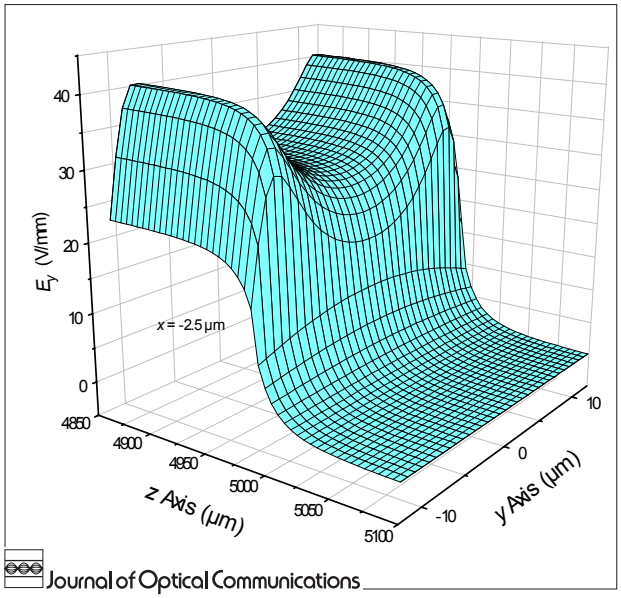

Fig. 4: Electric field distribution of $E_y(x,y,z)$ component on the plane [x = –2.5 μm] of an electrooptic phase modulator (SCPS, Y-cut) along the electrodes. (w = 40 μm, h_s = 0.0 μm L = 10 mm, h = 0.5 mm, ΔV = 1 V). The behavior of the $E_x(x,y,z)$ component is similar

has a strong influence on E_x component in contrast to the case of the E_y component. This behaviour is attributed to the direct dependence of the normal component E_x on the electrodes charge density.

Field calculations for a Z-cut electrooptic structure with a SiO_2 buffer layer between the electrodes and the substrate shown that the y component of the electric field pass continuously through the dielectric interface $x = -h_s$, while the field component E_x exhibits a large discontinuity equals to the ratio $\varepsilon_{x3}/\varepsilon_s$. In all cases the field strength in the region of optical waveguides decreases with increasing buffer layer thickness h_s, thus decreasing the electrooptical effect as well.

Once the charge density is available, it is easy to calculate the capacitance C, the characteristic impendence Z of the device and the effective permittivity ε_m for the guided electric wave. These parameters are very important in the design of electrooptical devices. Electrodes with a proper designed Z can achieve a good matching between the load and the microwave source, while the ε_m, which reflects how the electric waves are velocity matched to the optical waves, has a considerable influence on the modulation bandwidth and the efficiency of the electrooptical modulator or switch. According to the definitions of these parameters we have:

$$C = \frac{\iint_S \sigma(y,z)\,dydz}{\Delta V} \tag{7a}$$

Where ΔV is the voltage difference between the two electrodes (in ACPS or SCPS configuration) or between the central and the outer electrodes (in CPW configuration the outer electrodes are posed at the same voltage). The integration is performed on the surface of one electrode. By defining as C_0 the capacitance of the structure embedded in vacuum, the effective permittivity of the structure, the propagation constant β_m of electric waves travelling on the electrodes structure, and its characteristic impendence are given by the relations:

$$\varepsilon_m = \frac{C}{C_0}, \quad \beta_m = \frac{2\pi f}{c}\sqrt{\varepsilon_m}, \quad Z = \frac{\beta_m L}{2\pi f C} \tag{7b}$$

Calculations show that the capacitance of a given electrode configuration is almost the same for all crystal cuts provided that the thickness of the anisotropic substrate h is greater than 0.5 mm and the electrode length is greater than 1 mm. So, in all practical cases the parameters Z and ε_m are independent from the choice of the substrate orientation. Figure 5 shows a plot of the parameters C and Z for an ACPS structure as functions of the structural electrode ratios s/w_i for some values of the thick-

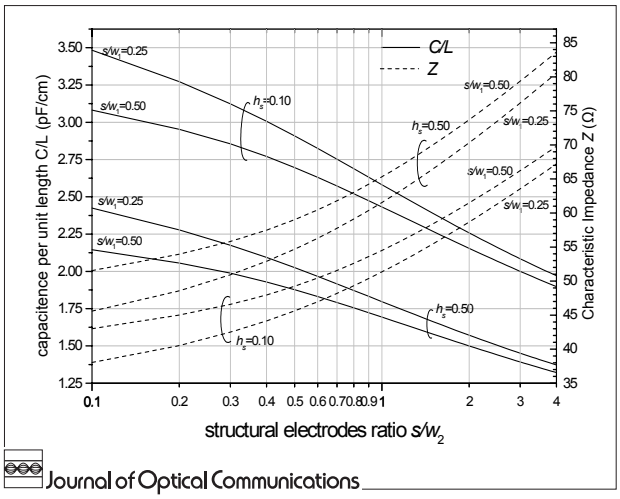

Fig. 5: Calculated capacitance per unit length and characterristic impedance of an electrooptic phase modulator (ACPS, Z-cut) and the influence of the SiO_2 buffer layer. (h = 0.5 mm, ΔV = 1 V)

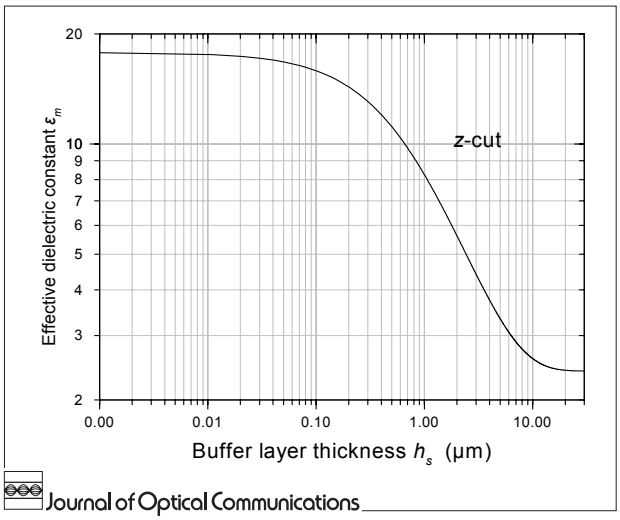

Fig. 6: Effective permittivity of a coplanar structure with two thin electrodes(ACPS Y or Z-cut) as a function of the buffer layer thickness (SiO_2, $\varepsilon_s = 3.8$)

ness h_s of the SiO_2 buffer layer. Notice that the parameter ε_m is not very sensitive to s/w_i owing to the assumption of thin electrodes.

However, εm is strongly dependent on hs as depicted in Fig. 6. An increase in h_s per 0.1 μm, results to decrease in ε_m of about 0.80. It is apparent that the effective dielectric constant ranges from the value $(1 + \sqrt{\varepsilon_{x3}\varepsilon_{y3}})/2 = 17.85$ for $h_s = 0$ to the value $(1 + \varepsilon_s)/2 = 2.4$ for $h_s \to \infty$. All the results confirm the consistency of the IM to the other methods [1, 2, 12].

Although the presented Integral Method is computational tedious, it results to a cohesive formulation including most electrooptic structures, and is well suited for computer solution, retaining the physical insight of the problem. In addition, as it will be seen in the next section, this static version of IM is easily extended to higher frequencies, while the effect of the electrodes thickness is taken into account in a very simple manner.

3 The effect of the electrode thickness. Extension to high frequencies and conductor losses estimation

Present practice for the fabrication of high bandwidth electrooptic devices is to use thick (3–15 μm) electrodes to satisfy the velocity matching conditions for the optical and microwave control waves. Therefore in order to achieve a more accurate modelling of practical electrooptic devices the finite electrode thickness t must be taken into account.

The electric field just outside the plane of the electrodes (x = 0) is nearly parallel to the y-axis and depends mainly on the electrodes voltage difference. The electric field in the substrate is determined by the boundary conditions at x = 0, which always are $E_y = 0$ at the electrode surfaces and $E_x = 0$ outside, regardless of the value of t.

As a result the electric field in the substrate for the case of thick electrodes is nearly the same as that in the case of the infinitely thin electrodes. Hence, the calculations presented in the previous section consist a very good approximation. Despite this fact, the values of the remaining electrical parameters are not accurate enough for the design purposes especially when t is large. In order to avoid complicate calculations the excess capacitance ΔC_t, due to the thickness of the electrodes, is considered to be equivalent to a parallel plate capacitor formed by the side walls of the thick electrode across the air gap and it is simply added to the capacitance given by (7a). The excess capacitance (in F/m) is approximated by the semiempirical relation [4]:

$$\Delta C_t = 2\pi\varepsilon_0 \frac{a_1 + a_2 \ln(s/w) + a_3 \ln(a_4 + t/s)}{\ln(4s/t) + 0.125(t/s)^2} \tag{8a}$$

Where w is the width of the signal electrode, $a_1 = 0.56667$, $a_2 = 0.03834$, $a_3 = 0.22411$, $a_4 = 0.08893$ for ACPS or SCPS and $a_1 = 0.49254$, $a_2 = 0.01709$, $a_3 = 0.21918$, $a_4 = 0.10357$ for CPW electrode configuration. Introducing a correction factor δ_c:

$$\delta_c = 1 + \frac{\Delta C_t}{C} L \tag{8b}$$

the capacitance C_t, the characteristic impendence Z_t and the effective permittivity ε_{mt} of the device in the case where the electrode thickness is not negligible (t/s > 0.1) are approximated as follows:

$$\left.\begin{aligned} C_t &= \delta_c C \\ Z_t &= Z \frac{1}{\sqrt{\delta_c\left[\varepsilon_m(\delta_c - 1) + 1\right]}} \\ \varepsilon_{mt} &= \varepsilon_m \frac{\delta_c}{\varepsilon_m(\delta_c - 1) + 1} \end{aligned}\right\} \tag{8c}$$

while C, Z, ε_m are still obtained from relations (7).

As it is apparent from the above relations the characteristic impendence and the effective permittivity decrease as the electrode thickness is increased. This behavior is explained qualitatively by the fact that the extension of the electrodes into air causes a no negligible part of the control microwave field to propagate in air. Furthermore, in

Journal of Optical Communications
24 (2003) 895

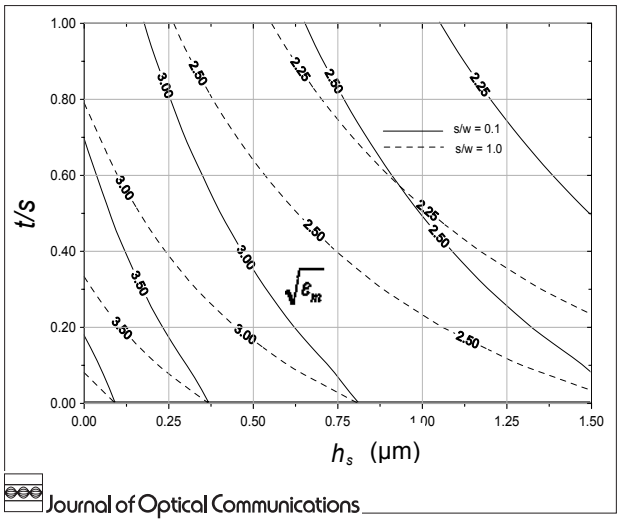

Fig. 7: Contour plots of the effective microwave refractive index of a coplanar structure (ACPS Y or Z-cut) on the [h_s, t/s] plane with the electrode structural ratio s/w as parameter

Fig. 7 contour plots of the effective microwave refractive index $\sqrt{\varepsilon_m}$ on the [h_s, t/s] plane are shown. Additionally a dependence of ε_m on the electrode structural ratio s/w is now revealed. It is therefore deduced that, a combination between the electrodes and the buffer layer thickness can effectively control the characteristics of an electrooptic device.

For a $LiNbO_3$ substrate ($\varepsilon_m \approx 17.85$) and for typical electrode transverse dimensions (≈ 100 μm), the upper limit of the frequency range over which the static approximation is valid is estimated to be about 60 GHz. This is a fact confirmed by using dynamic full wave methods and by experiments [1, 2]. Concerning the longitudinal direction, provided that the typical lengths of the electrooptic devices are about 1 cm, the static approximation is valid up to 0.6 GHz. However, at higher frequencies the electrodes of an electrooptic device behave like a transmission line with characteristic parameters approximated by the relations (8). The control microwave signal applied to electrodes, is then corresponding to a quasi TEM wave with propagation constant $\gamma_m = a_m + j\beta_m$, where β_m is the phase constant determined by (7c) and (8b) and a_m is the attenuation factor. Considering a sinusoidal electric drive voltage $V_G e^{j\omega t}$, the voltage seen along the electrode by the guided optical mode, can be written as:

$$V(z,t) = V_G \frac{Z\left(e^{-\gamma_m z} + \rho_T e^{-2\gamma_m L} e^{+\gamma_m z}\right) e^{j\omega\left(t - \frac{L-z}{c} n_k\right)}}{\left(R_G + Z\right)\left(1 - \rho_T \rho_G e^{-2\gamma_m L}\right)} \quad (9a)$$

Where R_G is the internal resistance of the microwave generator ($\approx 50\ \Omega$), ρ_G and ρ_T are the reflection coefficients of the transmission line at the edge of the source and the load resistance Z_T respectively, while n_k is the refractive index of the optical mode, depending on its polarization (k = x, y for TM, TE polarized wave respectively).

The effective voltage seen by the optical mode along the electrodes is:

$$\overline{V}(\omega,t) = \frac{1}{L}\int_0^L V(z,t)\,dz \quad (9b)$$

In the typical case of the travelling wave electrodes (TW), Z_T is chosen so that the equivalent to the electrodes transmission line will be perfectly terminated ($Z_T = Z$, $\rho_T = 0$). The relation (9a) is quite simplified, and the amplitude of the effective voltage is given by:

$$\overline{V}(\omega) = V_0 H(\omega) \quad (9c)$$

Where,

$$\left.\begin{aligned} H(\omega) &= e^{\frac{a_m L}{2}} \sqrt{\frac{\sinh^2\left(\frac{a_m L}{2}\right) + \sin^2\left(\omega \frac{\sqrt{\varepsilon_m} - n_k}{2c} L\right)}{\left(\frac{a_m L}{2}\right)^2 + \left(\omega \frac{\sqrt{\varepsilon_m} - n_k}{2c} L\right)^2}} \\ V_0 &= \frac{Z}{R_G + Z} V_G \end{aligned}\right\} \quad (9d)$$

Obviously V_0 is the dc voltage applied to the electrodes (i.e. the static voltage for which the calculations presented in the previous sections have been performed). The frequency function H(ω) can be seen as the transfer function of the structure, taking into account the propagation characteristics of the microwave signal and its velocity mismatch to optical mode.

Regarding the attenuation, the losses due to dielectric substrate are negligible compared to the conductor losses due to the skin effect in the electrodes. The latter, for typical electrode dimensions at high frequencies (f > 0.6 GHz), is calculated using the incremental inductance formula [4]:

$$\left.\begin{aligned} a_m &= a_0 \sqrt{f} && \left[\mathrm{dBcm^{-1}}\right] \\ a_0 &= 8.686 \frac{\sqrt{\pi \varepsilon_0 / \sigma}}{Z}\left(\frac{\partial Z_0}{\partial s} - \frac{\partial Z_0}{\partial w} - \frac{\partial Z_0}{\partial t}\right) && \left[\mathrm{dBcm^{-1}G^{z^{-\frac{1}{2}}}}\right] \end{aligned}\right\} \quad (10)$$

where Z_0 is the free space characteristic impendence of the metal electrodes and σ is the metal conductivity. The derivative of Z_0, $\partial Z_0/\partial p$, p = s, w, t with respect to incremental recession of electrode surfaces are calculated numerically using (6) and (7). It is apparent from (10), that the conductor losses are depended on the electrodes configuration, on the existence of the buffer layer, the frequency f, and are independent from crystal-cut choice.

As it is depicted in Fig. 8, a loss reduction is expected when asymmetric electrodes are used. In all cases significant loss reduction is accomplished, increasing the thickness of the electrodes. In the same figure results of the losses factor are compared with corresponding experimental data. Although a discrepancy between them is evident which is mainly caused by the irregularities and defects of the actual conductor surfaces, the accuracy of approximation (8) is considered satisfactory at least in the range 0.05–40 GHz, where dielectric and radiation losses (proportional to f) can be omitted.

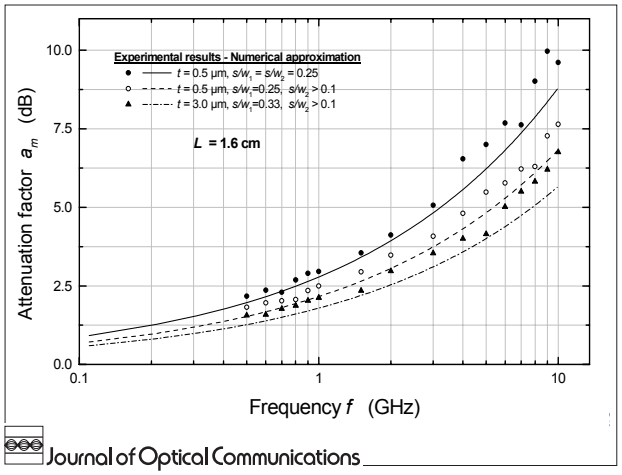

Fig. 8: Influence of the electrodes geometry of a coplanar structure (Y-cut ACPS or SCPS) on the conductor losses as a function of frequency (A_l electrodes, $\sigma_{Al} = 3.56\ 10^5$ mho/cm). The dispersion points denote experimental data [11]

So far an analysis concerning the microwave characteristics of the electrooptic devices has been presented. The evaluation of the operational parameters (half wave voltage Vπ, microwave drive power) of these devices requires the calculation of the guided optical field profile as well, which follows in the next section.

4 The optical mode profile in Ti diffused $LiNbO_3$ waveguides

The most common process for waveguide formation in $LiNbO_3$ devices is realized by Titanium (Ti) indiffusion into the crystal. So, in this work only this fabrication method is considered. The Ti indiffusion increases the substrate refractive index n_s in the waveguide area, creating waveguiding conditions. The realized index change profile $\Delta n(x,y)$ depends on the diffusion conditions and can rigorously be described by a quite complicated expression involving both the exponential and the error functions [6]. However, in typical situation $\Delta n(x,y) \ll n_s$, the conditions of weakly guidance are satisfied. Considering only the region of high density of the optical field, the refractive index profile is assumed elliptical in cross section and $\Delta n(x,y)$ is approximated by:

$$\Delta n(x,y) = \Delta n_0 \left[1 - \frac{(x - \Delta x_0)^2}{D_x^2} - \frac{(y - \Delta y_0)^2}{D_y^2} \right] \tag{11a}$$

where Δn_0 indicates the maximum change of the refractive index at the center of the waveguide, Δx_0, Δy_0 are the waveguide offsets from the coordinate origin and $D_{x,y}$ are the diffusion lengths along the x, y axes. Consequently the optical waveguide refractive index n_g is defined by:

$$n_g^2(x,y) = \begin{cases} n_s^2 + 2n_s \Delta n(x,y), & x \le 0, \quad \Delta n(x,y) \le 1 \\ n_s^2 & x \le 0, \quad \Delta n(x,y) > 1 \\ 1 & x > 0 \end{cases} \tag{11b}$$

Since $LiNbO_3$ is birefringent, the values of the parameters n_s, Δn_0, $D_{x,y}$ depend both on the polarization of the optical wave and on the crystal cut.

It is well known that the fields in weakly guiding waveguides are very nearly polarized (quasi TE or TM). Hence the strong field component of the waveguided optical signal (with propagation constant β), would have the form:

$$\Psi(x,y,z) = T(x,y) e^{-j\beta z} \tag{12a}$$

The function T(x,y) satisfies the scalar wave equation:

$$\frac{\partial^2}{\partial x^2} T(x,y) + \frac{\partial^2}{\partial y^2} T(x,y) + \left[k_0^2 n_g^2(x,y) - \beta^2 \right] T(x,y) = 0 \tag{12b}$$

In the above equation, $k_0 = 2\pi/\lambda =$, where λ is the optical wavelength in free space. In addition, the transverse field distribution satisfies the boundary condition $T(x,y) = 0$ at $x = 0$, since the electric fields of dielectric waveguides become very small at a large dielectric discontinuity. This is a reasonable assumption, since the upper to the optical waveguides layer includes the air and the metallic contacts (introducing losses) or just the buffer layer. By replacing (11b) into (12b), the resulting equation is of similar type to the equation of a harmonic oscillator in quantum mechanics and readily is resolved analytically, using separation of variables. The transverse spatial distribution of the fundamental mode follows as:

$$T(x,y) = A x \exp\left[-\left(\frac{(x - \Delta x_0)^2}{w_x^2} + \frac{(y - \Delta y_0)^2}{w_y^2} \right) \right] \tag{13a}$$

Thus, the fundamental mode of the diffused optical waveguide is approximated by a Hermite-Gaussian function, a fact confirmed experimentally. The parameters $w_{x,y}$ determine the cross-sectional shape of the optical mode, that is, the modal spot size. They are obtained by:

$$w_{x(y)}^2 = \frac{D_{x(y)}}{k_0} \sqrt{\frac{2}{n_s \Delta n_0}} \tag{13b}$$

The 1/e intensity full widths $\overline{w}_x$, $\overline{w}_y$ determine the more convenient geometric mean diameter $w_0 = \sqrt{\overline{w}_x \overline{w}_y}$ and the eccentricity $e_c = \overline{w}_y / \overline{w}_x$ of the optical mode. As it is clearly shown by the above relations, the mode size and symmetry are depended on the structural waveguide parameters, the orientation of the substrate and the optical wavelength considered. The parameter A is normalization constant, in order to have

$\int_{-\infty}^{+\infty} \int_{-\infty}^{0} T^2(x,y)\,dxdy = 1$ and follows as:

$$A^{-2} = \frac{\pi}{4} w_x w_y \left(\Delta x_0^2 + \frac{w_x^2}{4} \right) \left[1 + \mathrm{erf}\left(\frac{\sqrt{2}\Delta x_0}{w_x} \right) \right] + \sqrt{\frac{\pi}{2}} \frac{w_x^2 w_y \Delta x_0}{4} \exp\left[-2 \left(\frac{\Delta x_0}{w_x} \right)^2 \right] \tag{13c}$$

Journal of Optical Communications
24 (2003) 895

Table 1: Structural parameters for typical $LiNbO_3$ diffused waveguides. w, τ are the width and thickness of the diffused Ti strip and T, t are the temperature and the diffusion time

	cut	w(μm)	τ (nm)	T (°C)	t (h)
wg1 [12]	Z	4.00	80.0	1025	6.0
wg2[4]	Z	2.75	120.0	1050	3.2
wg3[8]	Z	4.00	100.0	1050	6.0
wg4[4]	Y	6.56	112.5	1059	2.0
wg5 [9]	Y	5.00	50.0	1020	9.0

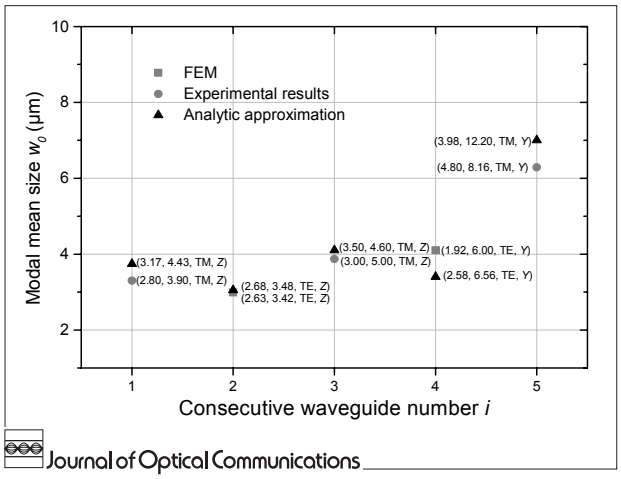

Fig. 9: comparison of the optical mode mean size w_0 for some typical diffused waveguide sin $LiNbO_3$. The parameters of each mode are shown as ($\overline{w}_x$, $\overline{w}_y$, Polarization, crystal cut)

The accuracy of the model is confirmed for a set of typical diffused waveguides [wg_i], comparing its results to experimental ones and to those obtained by the more accurate Finite Elements Method (FEM). The diffusion parameters of the waveguides are shown in Table 1, while in all cases $\lambda = 1.3$ μm.

The operational characteristics of the electrooptic devices are mainly depended on the spot size of the modal field, and consequently the mean size w_0 is compared in each case. The results are shown in Fig. 9 and the observed discrepancies do not exceed 5% (for Z-cut substrates) or 15% (for Y-cut substrates). Note that the dispersive parameters n_s, Δn_0 have been corrected in our calculations, using correction factors obtained by interpolation of experimental data [7].

Concluding, the approximate analytical solution takes into account all the waveguide fabrication parameters and it can be used to design electrooptic devices with accuracy and much less computational effort. To our knowledge this approach is applied for first time into the study of the diffused electrooptic waveguides.

The modal properties are also strongly depended on the orientation of the substrate. In Figure 10 illustrative plots to convey an impression of the appearance of the guided mode are shown.

The diffusion conditions resulting an optical single mode waveguide for $\lambda = 1.3$ μm and for both substrate cuts are found in [9]. It is obvious that in the Z-cut substrates, the fundamental modes (TM or TE) are more confined

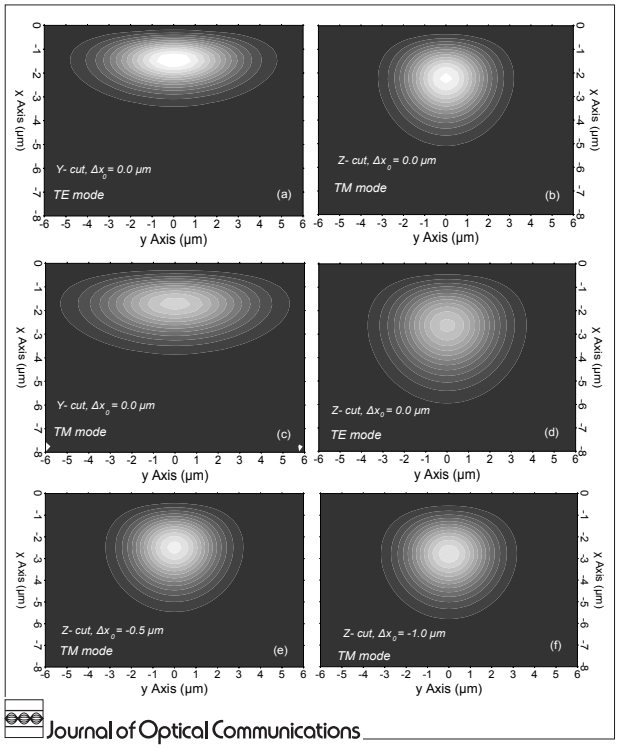

Fig. 10: Calculated intensity contour plots of the fundamental optical mode (TE or TM) propagated in Ti diffused waveguide on Y or Z-cut $LiNbO_3$ substrate

than the respective ones in Y-cut, due to the diffusion anisotropy of the latter. As the waveguide approaches the substrate surface ($\Delta x_0 \rightarrow 0$) the field distribution becomes deformed especially for the TE mode.

This fact implies that the coupling efficiency to the optical fiber is reduced. The field distribution of the modes becomes more symmetrical with increasing Δx_0. Unfortunately in this case the strength of the control electric field under the electrodes is also reduced. Hence, in typical case, large distances of the optical waveguide from the crystal surface are not preferred. Consequently only the offset imposed by the buffer layer is taken into account.

5 Performance and design considerations

The control process of an electrooptical device is accomplished by the linear electrooptic effect (Pockels). An external electric field applied to the device electrodes changes the refractive index of the optical waveguides, formed into the electrooptic substrate. As a result, a variation in the phase of the propagated optical beam is induced. For a sinusoidal microwave control signal $V_G e^{j\omega t}$, the total phase shift $\Delta\Phi$ is given by:

$$\Delta\Phi = \pi\delta_{mk}(\omega) \qquad k = x, y \tag{14a}$$

$$\delta_{mk}(\omega) = \delta_{mk0} H(\omega) \tag{14b}$$

In the above expressions $\delta_{mk}(\omega)$ is the frequency depended index modulation of the device, k denotes the polarization direction of the propagated optical mode, $H(\omega)$ is the transfer function defined by (10d), and δ_{mk0} is the static index modulation, defined as:

$$\delta_{mk0} = \frac{n_k^3}{\lambda}\bar{r}_k\Gamma_k\frac{V_0 L}{s} \qquad k = x, y \tag{15a}$$

V_0 is the dc voltage applied to the electrodes (9d), L the length and s the electrodes gap, λ the optical wavelength and Γ_k the normalized overlap factor between the microwave and optical waves, which can be derived by a perturbation analysis as:

$$\Gamma_k = \frac{s}{V_0 L}\int_{-L/2}^{L/2}\int_{0}^{-\infty}\int_{-\infty}^{\infty} E_k(x,y,z)\Gamma_J^2(x,y)\,dx\,dy\,dz \tag{15b}$$

Additionally in (15a), n_k is the refractive index of the substrate at optical frequencies and $\bar{r}_k$ appropriate coefficients, both depending on the polarization of the optical mode and the cut of the anisotropic substrate. In the case of a $LiNbO_3$ substrate:

$$\left.\begin{aligned} \bar{r}_{x(or\,y)} &= r_{33} \\ \bar{r}_{y(or\,x)} &= r_{22} + r_{13}\frac{\Gamma_{x(or\,y)}}{\Gamma_{y(or\,x)}} \\ n_{x(or\,y)} &= n_e \\ n_{y(or\,x)} &= n_o \end{aligned}\right\} Z(\text{or } Y)\text{cut} \tag{15c}$$

where $n_{o,e}$ are the ordinary and the extraordinary $LiNbO_3$ refractive index respectively and r_{ij} its electrooptic coefficients.

A very important operational parameter for electrooptical devices is the voltage length product for full modulation depth ($\delta_{mk0} = 1$):

$$[V_0 L]_\pi = \frac{\lambda}{n_1^3\bar{r}_k(\Gamma_k/s)} \qquad k = x, y \tag{16a}$$

By the assistance of this parameter, the drive power required by the microwave source of device to achieve full modulation depth at dc, may be written as:

$$P_{G(\pi)} = \frac{[V_0 L]_\pi^2}{2(1-\rho_G^2)ZL^2} \tag{16b}$$

As low drive power is usually required, the electrodes must be designed so that $Z \to R_G$, minimizing the reflection at the source side. In addition, one tries to minimize $[V_0L]_\pi$ by optimising the parameter Γ_k/s. In this optimisation it should be taken into account that a smaller s requires lower alignment tolerances for the optical waveguides. Furthermore, the overlap factor primarily depends on the relative position of the electrodes and the optical waveguides, as well as on the orientation of the substrate and the polarization of the optical mode.

The efficiency of an electrooptic device is strongly dependent on the buffer layer thickness, like the applied electric field E_k, and the spot size and shape of the propagating optical mode.

Our calculations show that the overlap factor Γ increases up to 10 % with decreasing the mean mode size w_0. This conclusion is independent from the choice of electrode parameters and only practical limitations to the fabrication of the diffused optical waveguide, assuring the existence of the proper number of modes in the devices, must be considered.

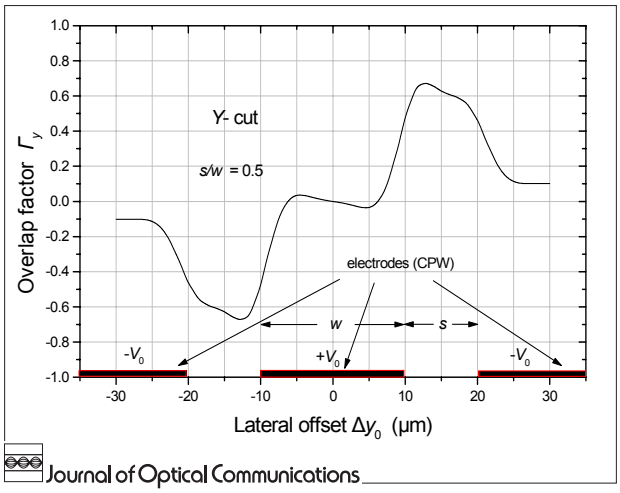

Fig. 11: Overlap integral factor for TE polarization (Y-cut $LiNbO_3$ and CPW electrodes, w_0 = 20 μm, L = 10 mm, h = 0.5 mm, s/w_0 = 0.5)

In practice the electrodes of the device are configured to provide push-pull operation. The presented analysis is easily extended to cover this situation, since only the overlap factor Γ_k in (16a) must simply be replaced by the sum $|\Gamma_{k1}| + |\Gamma_{k2}|$, where the subscripts 1 and 2 denote the optical waveguides used in this case. In Fig. 11 the parameter Γ_y for a typical CPW structure is shown. It is obvious that the optimum position for the optical waveguides is near the edges of the center electrode. In any case the push-pull configuration results an increment to parameter Γ_y by a factor of 2.

Representative results for the parameters δ_{mk0} and $[V_0L]_\pi$ of an SCPS typical structure are shown in Fig. 12. In each case, an intersection between the TE and TM curves is clearly seen. That is, for a certain placement of the optical waveguide relatively to the electrodes (offset Δy_0) the structure is polarization insensitive. However, in the case of Y-cut substrate, the required $[V_0L]_\pi$ product is too high to realized in practice. In the case of Z-cut a lower $[V_0L]_\pi$ product is expected. However, because of the large intersection angle, the placement of the optical waveguide has to be achieved with high accuracy (±0.5 μm). Therefore, technologically it seems to be easier to fabricate a polarization insensitive device by using two sets of electrodes (placed one after another) to modulate either TE or TM mode in an optimum manner.

The frequency response of an electrooptic device, is well determined by its transfer function H(ω), since its operational parameters are voltage depended. Assuming a small control signal the 3 dB electrical bandwidth of the device is determined by the frequency region $\Delta f = [0, f_0]$, with $H(2\pi f_0) = 0.707$. It can be seen from (9d), that the bandwidth depends on the conductor loss, the velocity mismatch between the optical and microwave signals measured by the term $\sqrt{\varepsilon_m} - n_k$, and decreases almost linearly with the electrode length L. Figure 13 illustrates contours of the parameter ΔfL on the $[a_0, \sqrt{\varepsilon_m}]$ plane. As $\sqrt{\varepsilon_m} \to n_k$ (≈ 2.2) for a given L, the bandwidth is increased and it is only limited by the conductor losses.

Journal of Optical Communications
24 (2003) 895

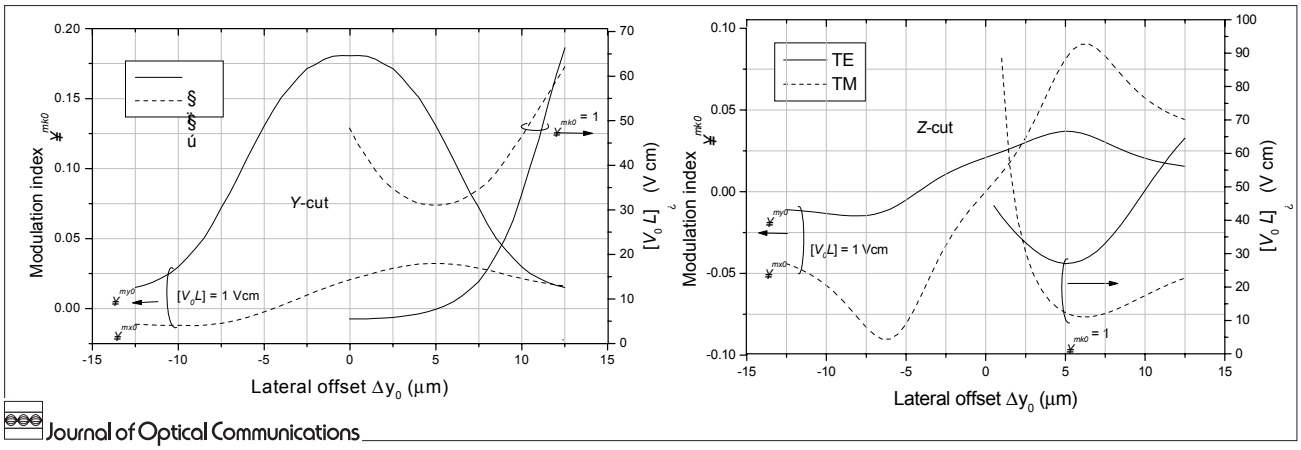

Fig. 12: Influence of the optical mode polarization and position into the operational parameters of an electrooptic device (SCPS, s = 10 μm, L = 10 mm, h = 0.5 mm, s/w = 0.5). a) Y-cut: TE (4.8 μm, 0.34) and TM (5.7 μm, 0.35), b) Z-cut: TE (5.8 μm, 0.7) and TM (4.9 μm, 0.77)

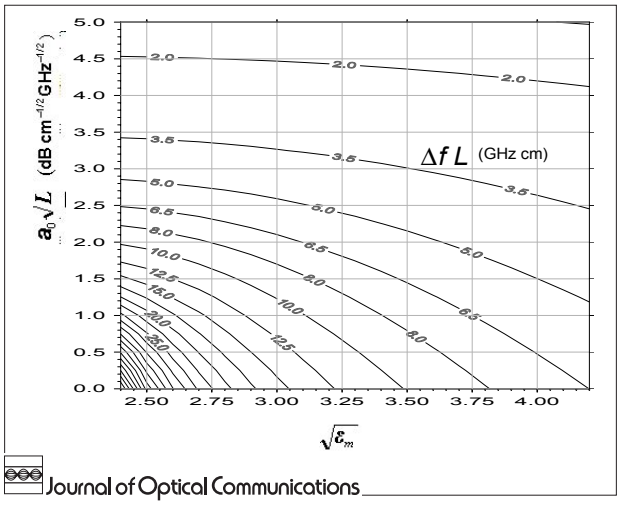

Fig. 13: Bandwidth contour plots for electrooptic devices with travelling wave (TW) electrodes

The increase the electrodes thickness t, can dramatically decrease the latter.

It can be calculated by (10), that increasing t from 3 μm to about 20 μm the losses coefficient a_0 is decreased by about 50 %. The calculated bandwidth Δf (for Z-cut, h_s = 0.8 μm) exceeds 75 GHz even for electrodes length greater than 4 cm. Unfortunately, by increasing t, the characteristic impedance of the electrodes decreases, resulting an appreciable part of the microwave control power to be reflected at the source side, as predicted by (16b).

In order to obtain reasonable values for drive power, the most promising technique is to groove the substrate region between the electrodes. In this way, the device impedance increases towards 50 Ω, and the advantage of thick electrodes is exploited with the cost of increasing the complexity of the fabrication process.

The presented model is used to calculate the operational parameters of some practical electrooptic devices, found in the literature with excellent agreement, shown in Table 2. The systematic slight deviation in the values of the bandwidth may be attributed to the underestimation of the conductor losses. The real values of V_π are greater than the calculated ones, since the optical mode in a real situation is not focused so tight as predicted by (13).

However, the presented model may be used in the design of electrooptic devices with an expected accuracy better than 10 % for their operational parameters.

The design considerations for broadband TW electrooptic devices must include: microwaveoptical velocity match, low conductor losses, a low V_π and an electrode characteristic impedance Z near 50 Ω to minimize the required microwave power $P_{G\pi}$. With any electrooptical material, it is difficult to concurrently satisfy all these requirements and hence tradeoffs are inevitable. Notice that the bandwidth is determined only by H(ω) independently of optical design, while the drive power depends both on Z and Γ_k. Since in the design of a device the goal is primarily the attainment of a specific bandwidth, the optimization problem is quite simplified. For a given Δf and optical waveguide parameters, various sets (L, w, s, t, h_s, Δy_0) are determined by an iterative procedure. Next the specific set, which results the minimum drive power calculated by (16b) is selected as the optimum device geometrical parameters. In addition the best optical waveguides parameters, which minimize the modal spot size, could be considered and a second iteration is performed. The iteration process continues until the desired accuracy of the each structural parameter is reached.

Table 3 summarizes the optimum parameters for an ACPS device that requires the minimum drive power for a 20 GHz bandwidth. The characteristics of the fundamental optical mode for each polarization are shown in Fig. 10. The gold electrodes have a thickness t = 3 μm, which is the maximum value achievable by conventional electroplating techniques. The design concept remains the same for devices with push pull (pp) configuration. In some cases (electrooptic intensity modulators), restrictions concerning the optical waveguides center-tocenter separation must be imposed, in order to avoid coupling effects between them. Although when the parameter s increases and the strength of the microwave electric field under the electrodes is decreased, a significant reduction in the required microwave drive power $P_{G\pi}$ is eventually accomplished, due to the push pull operation and the increase of the Γ_k. A further reduction (≈ 20 %) of $P_{G\pi}$

Table 2: Operational parameters of electrooptic phase modulators calculated by the Integral method and corresponding experimental ones

Device		Z (Ω)	V_π (V)	$\Delta f_{3dB\ el}$ (GHz)
wg_i : [w (μm), τ(nm), T (°C), t (h), λ (μm)] el_1: [w_1, w_2, L, t, s, h_s] (μm)				
wg_1: [8, 500, 1030, 6.0, 1.3]	Ex	40.0	4.00	3.60
el_1: [14, 60, 1.6 10^4, 3 (Al), 6.0, 0.0] [5]	IM	36.6	3.80	3.90
wg_2: [9, 78, 1050, 6.5, 1.55]	Ex	52.0	4.00	3.60
el_2: [13, 120, 0.5 10^4, 3 (Au), 23.0, 0.2] [11]	IM	51.5	4.00	3.85
wg_3: [4 , 100, 1050, 6.0, 0.6328]	Ex	49.8	9.60	7.70
el_3: [10, 100, 0.64 10^4, 1.5 (Au), 10.0, 0.1] [6]	IM	48.7	9.32	8.20

Table 3: Electrooptic phase modulators (ACPS-TW) with Δf = 20 GHz and optimum microwave drive power. In all cases: t = 3 μm (Au), h >500 μm, λ=1.3 μm

cut	s (μm)	w_1 (μm)	w_2 (μm)	h_s (μm)	L (cm)	Z (Ω)	V_π (V)	$P_{G(\pi)}$ (W)
Z (TM)	12.0	22.0	120.0	1.12	1.27	57.0	10.97	1.085
Z (TM) pp	17.6	36.0	175.0	1.18	1.31	58.4	7.42	0.472
Y (TE)	7.6	37.5	120.0	0.00	0.41	30.5	9.54	1.636

is occurred when optical modes having the tightest confinement are used. In this case the electrode parameters shown in Table 3 are slightly changed.

The electrodes on Z-cut substrates possess smaller microwave effective index than the electrodes on Y-cut, due to the buffer layer. Hence, reasonable values for the factor losses a0 can be achieved for even longer electrodes. On the other hand the Y-cut devices present the lowest parameter $[VL]_\pi$.

The higher impedance in Z-cut however, offsets this advantage gained by the larger Γ_k in Y-cut devices, which eventually have a significantly higher drive power requirement. These conclusions are general and hold independently of the configuration of the electrodes.

6 Conclusions

A numerical model for the evaluation of the microwave and optical characteristics of electrooptic devices has been presented. The model is quite general and applicable to most practical electrooptic devices (switches and modulators) used in the broadband optical networks. The 3-D analysis of the microwave control field reveals some differences between the Y-cut and Z-cut devices, which are negligible for long electrodes. Calculated values of microwave parameters indicate that both increasing the electrode and the buffer layer thickness results in a large bandwidth for a given electrode length. Considering the optical field analysis, a simple analytic solution of the wave equation for the fundamental mode has been presented. In spite of simplicity, significant differences between the TE and TM modes are revealed and taken into account by the model. The direct relation of the mode spot size to diffusion parameters is useful in optimization of the used optical waveguides. In addition an electrooptic polarization insensitive device seems to be more feasible on a Z-cut substrate.

The accuracy of the model is satisfactory compared to experimental results. Following the design procedure described above it is shown that electrooptic devices with conventional electrodes (t = 3 μm) and bandwidth up to 20 GHz are feasible. Higher bandwidths with reasonable drive power require thicker electrodes.

The level of detail and the generality of the presented numerical model make it a useful numerical tool in the evaluation and the design of electrooptic components, for present and future high-speed optical networks.

References

[1] J. Gerdes et al: “Full-wave analysis of traveling-wave electrodes with finite thickness for electro-optic modulators by the method of Lines”; IEEE J. Lightwave Tech. 9 (1991) 4, 461–467

[2] D. Marcuse: “Electrostatic field of coplanar lines computed with the point matching method”; IEEE J. Quantum Electron. 25 (1989) 6, 939–947

[3] T. Sphicopoulos et al: “Green function for the three – dimensional analysis of electrooptic modulators”; Applied Optics 30 (1991) 9, 3862–3866

[4] H. Chung et al: “Modeling and optimization of Traveling–Wave $LiNbO_3$ Interferometric Modulators”; IEEE J. Quantum Electron. 27 (1991) 3, 608–617

[5] K. Kubota et al: “Traveling–wave optical modulator using a directional coupler $LiNbO_3$ waveguide”; IEEE J. Quantum Electron. 16 (1980) 7, 754–760

[6] A. Sharma and P. Bindal: “Analysis of diffused planar and channel waveguides”; IEEE J. Quantum Electron. 29 (1993) 1, 150–153

[7] S. Fouchet et al: “Wavelength dispersion of Ti induced refrective index change in $LiNbO_3$ as a function of diffusion parameters”; IEEE J. Lightwave Technol. 5 (1987) 3, 700–708

[8] W. C. Chuang et al: “A comparison of the performance of the $LiNbO_3$ traveling-wave Phase modulators with various dielectric buffer layers”; J. Opt. Commun. 14 (1993) 4, 142–148

[9] H. Porte et al: “An $LiNbO_3$ Integrated Coherence Modulator”; IEEE J. Lightwave Technol. 10 (1992) 6, 760–766

[10] F. S. Chu and P. Liu, “Simulations of Ti diffused $LiNbO_3$ waveguide modulators – A comparison of simulation techniques”; IEEE J. Lightwave Technol. 8 (1990) 10, 1492–1496

[11] K. W. Hui et al: “Optical optimization for high speed traveling-wave Integrated Optic modulators”; IEEE J. Lightwave Technol. 16 (1998) 2, 232–238

[12] M. C Kim, and V. R Ramaswamy: “Overlap integral factors in integrated optic modulators and switches”; IEEE J. Lightwave Technol. 7 (1989)7, 1063–1070